Anharmonic Correction to Free Energy Barriers from DFT-Based Molecular Dynamics Using Constrained Thermodynamic Integration

Jonas Amsler,* Philipp N. Plessow, Felix Studt, and Tomáš Bučko*

ABSTRACT: For the calculation of anharmonic contributions to free energy barriers, constrained thermodynamic λ-path integration (λ-TI) from a harmonic reference force field to density functional theory is presented as an alternative to the established Blue Moon ensemble method (ξ-TI), in which free energy gradients along the reaction coordinate ξ are integrated. With good agreement in all cases, the λ-TI method is benchmarked against the ξ-TI method for several reactions, including the internal CH_3 group rotation in ethane, a nucleophilic substitution of CH_3Cl, a retro-Diels–Alder reaction, and a proton transfer in zeolite H-SSZ-13. An advantage of λ-TI is that one can use virtually any reference state to compute anharmonic contributions to reaction free energies or free energy barriers. This is particularly relevant for catalysis, where it is now possible to compute anharmonic corrections to the free energy of a transition state relative to any reference, for example, the most stable state of the active site and the reactants in the gas phase. This is in contrast to ξ-TI, where free energy barriers can only be computed relative to an initial state with all reactants coadsorbed. Finally, the Bennett acceptance ratio method combined with λ-TI is demonstrated to reduce the number of required integration grid points with tolerable accuracy, favoring thus λ-TI over ξ-TI in terms of computational efficiency.

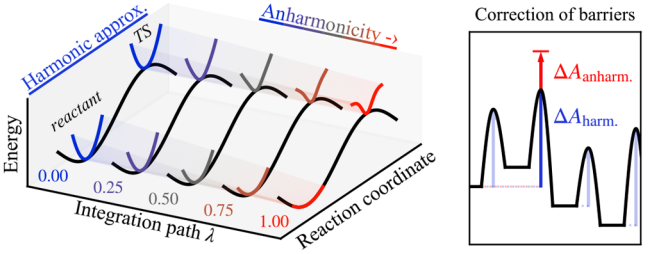

1. INTRODUCTION

The accurate quantification of anharmonicity on the molecular scale, defined as deviation from the harmonic oscillator approximation, represents one of the grandest challenges in computational heterogeneous catalysis, with particular relevance for supported metal nanoparticles, confinement effects in zeolites, and solid–liquid interfaces.[1,2] Disappointingly, despite the known significance of anharmonicity—oftentimes estimated on the basis of density functional theory (DFT) and molecular dynamics (MD)—relatively few studies provide more than a rough estimate for entropy and free energy contributions. In comparison, anharmonicity is relatively well explored for solid materials.[3−9]

Yet, free energies for anharmonic systems of catalytic relevance can be computed by several procedures. Typically, these procedures determine either the free energy of a single thermodynamic state locally or the free energy difference between two thermodynamic states by following the connecting continuous path on the free energy surface. In the former case, many procedures aim to improve the accuracy for stationary states on the potential energy surface. For use in the so-called static approach, which is based on local topology of the potential energy surface close to the stationary point of interest, approximations to the partition functions of hindered translators and hindered internal rotors for molecules and adsorbates have been developed[10−14] that avoid time-consuming explicit sampling of configuration space. Not only do these assumptions and simplifications require prior knowledge about the mobility of the system components, but their reliability also strongly depends on the thermodynamic conditions. For instance, a comparison of predictions by the harmonic oscillator, hindered, and free translator approximations with the complete potential energy sampling approach has shown that none of the simple approximations is reliable for modeling adsorbates over a wide range of temperatures.[15] Other ideas improve the harmonic oscillator approximation by adapting the force constants using quasi-harmonic or effective harmonic approximations.[4,16−19] In a rather involved correction to the static approach, anharmonic vibrational partition functions have been determined by solving one-dimensional Schrödinger equations defined for the potential energies explicitly sampled along individual vibrational eigenmodes expressed in terms of internal coordinates.[20−24] Thermodynamic integration (TI)[25−27] along temperature and Hamiltonian-based λ-paths[28−33] has been used to study crystalline systems[8,34−36] and phase transitions.[18,37−41] In particular, TI from Debye models to fully interacting crystalline systems[42,43] is conceptually similar to the

method reported in this work, where we present a more generally applicable TI method from harmonic reference systems to fully interacting DFT-based systems. Local methods for individual thermodynamic states aside, the second type of procedures computes free energy differences between two states using TI or similar schemes based on multistage sampling. Methods of this kind, like umbrella sampling[44−46] or the Blue Moon ensemble method described by Ciccotti et al.,[47−49] can be employed routinely to calculate free energy barriers under consideration of anharmonicity as simulated by DFT-based MD. While these methods are designed for the investigation of rare events, such as the event of passing through a transition state (TS) of a chemical reaction or phase transition, they also depend on contributions from intermediate states located along the reaction coordinate ξ connecting the reactant state and the TS. Thereby obtained free energy differences can hardly be referenced to arbitrary states outside the transformation path considered. For example, the calculation of a free energy barrier for a reaction near the end of an extended reaction cascade relative to the state of the initial reactants would require integration along all reactions from the beginning to that barrier, which is very time-consuming and exhibits an unfavorable accumulation of the statistical error, which increases with the length of the path taken.[50]

To calculate the anharmonic correction to the harmonic approximation for adsorption free energy, we have reported a method harnessing thermodynamic λ-path integration (λ-TI) of DFT-based MD using curvilinear coordinates. Instead of integrating along the reaction coordinate ξ, λ-TI integrates along a progressive parameter λ that couples a harmonic reference force field with DFT. This independence from a continuous path on the free energy surface makes λ-TI also interesting when applied to reaction barriers; for example, selected barriers in an expanded reaction network could be corrected by anharmonic contributions relative to arbitrary reactant states. To this end, we now demonstrate how our λ-TI method can be applied to the constrained ensemble of a TS. We furthermore present λ-TI as an alternative to the established Blue Moon ensemble method,[47−49] which we dub ξ-TI to emphasize its similarity to the λ-TI method presented in this work. For simple reactions with known ξ, the λ-TI and ξ-TI methods are directly compared. The overall aim of this study is to show how to extract a free energy barrier—a fundamental property bearing information on the reaction rate—using the λ-TI method. Finally, an unorthodox application of the Bennett acceptance ratio (BAR) method[51,52] is demonstrated to eliminate the number of required integration grid points with tolerable accuracy.

2. METHODS

2.1. Summary of the Thermodynamic λ-Path Integration in Internal Coordinates. In this section, we briefly recapitulate the thermodynamic λ-path integration (λ-TI) method with a harmonic reference, formulated in terms of internal coordinates that we introduced in our previous work.[53] We motivated our choice of the harmonic reference system through the popularity of the harmonic approximation in heterogeneous catalysis and adsorption thermodynamics.[21−23,54−59]

For a fully interacting system 1, we express its Helmholtz free energy A_1 as

$$A_1 = A_{0,\boldsymbol{x}} + \Delta A_{0,\boldsymbol{x}\to 1} \tag{1}$$

where $A_{0,\boldsymbol{x}}$ is the free energy of a reference system 0 being harmonic in Cartesian coordinates $\boldsymbol{x}$ and $\Delta A_{0,\boldsymbol{x}\to 1}$ is the remaining difference, defined as

$$\Delta A_{0,\boldsymbol{x}\to 1} = -k_\mathrm{B}T \ln\left[\frac{Q_1}{Q_{0,\boldsymbol{x}}}\right] \tag{2}$$

In eq 2, $Q_\alpha = M\int \mathrm{d}\boldsymbol{p}\ \mathrm{d}\boldsymbol{q}\ \exp(-\mathcal{H}_\alpha/k_\mathrm{B}T)$ is the partition function of system α defined by Hamiltonian $\mathcal{H}_\alpha$, M is a normalization constant common to both systems (but otherwise irrelevant for the present discussion), T is the temperature, and k_B is the Boltzmann constant. As discussed in our previous work,[53] the harmonic reference system can be chosen arbitrarily and does not necessarily coincide with the true harmonic approximation of the state at hands. This choice will, however, influence the sampling efficiency. We derive the harmonic reference system from the Hessian matrix obtained through finite differences in $\boldsymbol{x}$ at the DFT level of theory, and, for numerical reasons, we increase all eigenvalues lower than a certain limit, typically 1 or 2 eV·Å^{-2}, to that limit while preserving the original eigenvectors. In this work, the quasi-classical free energy expression for the harmonic reference system was used, expressed as[60]

$$A_{0,\boldsymbol{x}} = A_\mathrm{el}(\boldsymbol{x}_0) - k_\mathrm{B}T\sum_{i=1}^{N_\mathrm{vib}} \ln\frac{k_\mathrm{B}T}{\hbar\omega_i} \tag{3}$$

where $A_\mathrm{el}(\boldsymbol{x}_0)$ is the electronic free energy for the minimum energy configuration of the reference system with atomic position vector $\boldsymbol{x}_0$, N_vib represents the number of vibrational modes i with real angular frequencies ω_i, and $\hbar$ is the Planck constant divided by 2π. We chose the quasi-classical expression to ensure consistency with the benchmark ξ-TI method that utilizes DFT-based MD with classical nuclear degrees of freedom. We note, however, that the quantum mechanical formula[61] for $A_{0,\boldsymbol{x}}$ can be a more suitable choice in some applications, like reactions at very low temperatures.

Introducing a second reference system that is harmonic in rotationally and translationally invariant internal coordinates $\boldsymbol{q}$ with free energy $A_{0,\boldsymbol{q}}$, we express $\Delta A_{0,\boldsymbol{x}\to 1}$ according to

$$\Delta A_{0,\boldsymbol{x}\to 1} = \Delta A_{0,\boldsymbol{x}\to 0,\boldsymbol{q}} + \Delta A_{0,\boldsymbol{q}\to 1} \tag{4}$$

The relations between the true harmonic approximation (HA) to the free energy, the free energies of the reference systems harmonic in $\boldsymbol{x}$ and $\boldsymbol{q}$, and the anharmonic system are illustrated in Scheme 1. The terms $\Delta A_{0,\boldsymbol{x}\to 0,\boldsymbol{q}} = A_{0,\boldsymbol{q}} - A_{0,\boldsymbol{x}}$ and $\Delta A_{0,\boldsymbol{q}\to 1} = A_1 - A_{0,\boldsymbol{q}}$ can be obtained from

$$\Delta A_{\alpha\to\beta} = \int_0^1 \mathrm{d}\lambda\ \langle V_\beta - V_\alpha\rangle_\lambda \tag{5}$$

using numerical integration over the coupling parameter λ with one MD simulation per grid point. The placeholders are $\alpha = 0,\boldsymbol{x}$ and $\beta = 0,\boldsymbol{q}$ for the transformation between harmonic force fields, or $\alpha = 0,\boldsymbol{q}$ and $\beta = 1$ for the transformation between the system harmonic in $\boldsymbol{q}$ and the fully interacting system. The term $\langle\cdots\rangle_\lambda$ stands for the NVT ensemble average of the enclosed quantity, given by the Hamiltonian

$$\mathcal{H}_\lambda = \lambda\mathcal{H}_\beta + (1-\lambda)\mathcal{H}_\alpha \tag{6}$$

Corresponding to just a force field-to-force field transformation requiring no extra quantum mechanical calculations, the free

Scheme 1. Relations between the Electronic Free Energy of the System, Its True Harmonic Free Energy (Harmonic Approximation), and the Free Energies of the Reference States Harmonic in Cartesian ($A_{0,x}$) and Internal ($A_{0,q}$) Coordinates, and of the Anharmonic System[a]

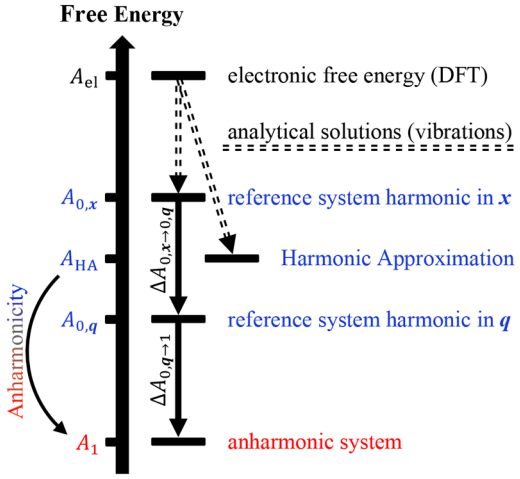

[a]With the assumption of harmonicity in Cartesian coordinates, analytical expressions for the free energy contributions in $A_{0,x}$ and A_{HA} are available (see eq 3).

energy difference between the two harmonic reference systems, $\Delta A_{0,x\to0,q}$, can be computed numerically at low cost. Moreover, this contribution is typically (but not always) small[53] and can often be neglected.

The harmonic reference system with Hessian matrix $\underline{\boldsymbol{H}}^{\boldsymbol{x}}$, determined as described above, is used to compute ω_i in eq 3 as well as the harmonic force fields

$$V_{0,\boldsymbol{x}}(\boldsymbol{x}) = V_{0,\boldsymbol{x}}(\boldsymbol{x}_0) + \frac{1}{2}(\boldsymbol{x}-\boldsymbol{x}_0)^{\mathrm{T}}\underline{\boldsymbol{H}}^{\boldsymbol{x}}(\boldsymbol{x}-\boldsymbol{x}_0) \tag{7}$$

and

$$V_{0,\boldsymbol{q}}(\boldsymbol{q}) = V_{0,\boldsymbol{q}}(\boldsymbol{q}_0) + \frac{1}{2}(\boldsymbol{q}-\boldsymbol{q}_0)^{\mathrm{T}}\underline{\boldsymbol{H}}^{\boldsymbol{q}}(\boldsymbol{q}-\boldsymbol{q}_0) \tag{8}$$

The Hessian matrices in $\boldsymbol{x}$ and $\boldsymbol{q}$ are related via the transformations

$$\underline{\boldsymbol{H}}^{\boldsymbol{x}} = \underline{\boldsymbol{B}}_{\boldsymbol{x}_0}^{\mathrm{T}}\underline{\boldsymbol{H}}^{\boldsymbol{q}}\underline{\boldsymbol{B}}_{\boldsymbol{x}_0} \tag{9}$$

and

$$\underline{\boldsymbol{H}}^{\boldsymbol{q}} = \underline{\boldsymbol{A}}_{\boldsymbol{x}_0}^{\mathrm{T}}\underline{\boldsymbol{H}}^{\boldsymbol{x}}\underline{\boldsymbol{A}}_{\boldsymbol{x}_0} \tag{10}$$

valid for stationary points ($\boldsymbol{x}_0$ and, correspondingly, $\boldsymbol{q}_0 = \boldsymbol{q}(\boldsymbol{x}_0)$), where $\underline{\boldsymbol{B}}$ and $\underline{\boldsymbol{A}}$ are the Wilson B-matrix[62] $\left(\underline{\boldsymbol{B}}_{ij} = \frac{\partial q_i}{\partial x_j}\right)$ and its Moore–Penrose pseudo-inverse, respectively.[62,63]

2.2. Harmonic Reference Systems with Holonomic Constraints. Now we introduce a harmonic reference system with one holonomic constraint $\xi(\boldsymbol{x}) = \xi'$. Note that the procedure described here can be generalized to systems with multiple independent constraints in a straightforward manner. First, let us express the ratio $\frac{Q_\beta}{Q_\alpha}$ as

$$\begin{aligned}\frac{Q_\beta}{Q_\alpha} &= \frac{\int \mathrm{d}\boldsymbol{p}\,\mathrm{d}\boldsymbol{q}\,\delta(\xi(\boldsymbol{q})-\xi')\exp(-\mathcal{H}_\beta/k_\mathrm{B}T)}{\int \mathrm{d}\boldsymbol{p}\,\mathrm{d}\boldsymbol{q}\delta(\xi(\boldsymbol{q})-\xi')\exp(-\mathcal{H}_\alpha/k_\mathrm{B}T)} \times \\ &\quad \frac{\int \mathrm{d}\boldsymbol{p}\,\mathrm{d}\boldsymbol{q}\delta(\xi(\boldsymbol{q})-\xi')\exp(-\mathcal{H}_\alpha/k_\mathrm{B}T)}{\int \mathrm{d}\boldsymbol{p}\,\mathrm{d}\boldsymbol{q}\delta(\xi(\boldsymbol{q})-\xi')\exp(-\mathcal{H}_\beta/k_\mathrm{B}T)} \times \frac{Q_\beta}{Q_\alpha} \\ &= \frac{\int \mathrm{d}\boldsymbol{p}\,\mathrm{d}\boldsymbol{q}\,\delta(\xi(\boldsymbol{q})-\xi')\exp(-\mathcal{H}_\beta/k_\mathrm{B}T)}{\int \mathrm{d}\boldsymbol{p}\,\mathrm{d}\boldsymbol{q}\,\delta(\xi(\boldsymbol{q})-\xi')\exp(-\mathcal{H}_\alpha/k_\mathrm{B}T)} \times \frac{P_\alpha(\xi')}{P_\beta(\xi')}\end{aligned} \tag{11}$$

where the term $P_i(\xi') = \frac{\int \mathrm{d}\boldsymbol{p}\,\mathrm{d}\boldsymbol{q}\,\delta(\xi(\boldsymbol{q})-\xi')\exp(-\mathcal{H}_i/k_\mathrm{B}T)}{Q_i}$ represents the probability density of ξ in the NVT ensemble driven by Hamiltonian $\mathcal{H}_i$. As before, the placeholders are $\alpha = 0,\boldsymbol{x}$ and $\beta = 0,\boldsymbol{q}$ for the transformation between harmonic force fields, or $\alpha = 0,\boldsymbol{q}$ and $\beta = 1$ for the transformation between the system harmonic in $\boldsymbol{q}$ and the fully interacting system. Upon inserting the final formula from eq 11 into eq 2, we obtain the following useful expression:

$$\Delta A_{\alpha\to\beta} = \Delta A_{\alpha\to\beta}(\xi') - k_\mathrm{B}T\ln\left[\frac{P_\alpha(\xi')}{P_\beta(\xi')}\right] \tag{12}$$

The term $\Delta A_{\alpha\to\beta}(\xi') = -k_\mathrm{B}T\ln\left[\frac{\int \mathrm{d}\boldsymbol{p}\,\mathrm{d}\boldsymbol{q}\,\delta(\xi(\boldsymbol{q})-\xi')\exp(-\mathcal{H}_\beta/k_\mathrm{B}T)}{\int \mathrm{d}\boldsymbol{p}\,\mathrm{d}\boldsymbol{q}\,\delta(\xi(\boldsymbol{q})-\xi')\exp(-\mathcal{H}_\alpha/k_\mathrm{B}T)}\right]$ is the free energy difference between the systems α and β with $\xi(\boldsymbol{x})$ fixed at the value ξ'. This term can be obtained in constrained λ-TI MD simulations using the SHAKE algorithm:[64]

$$\Delta A_{\alpha\to\beta}(\xi') = \int_0^1 \mathrm{d}\lambda\,\frac{1}{\langle Z^{-1/2}\rangle_{\lambda,\xi'}}\langle Z^{-1/2}(V_\beta - V_\alpha)\rangle_{\lambda,\xi'} \tag{13}$$

Equation 13 results from eq 5 by applying the following relation[47] between the unconstrained ($\langle O\rangle$) and the constrained ($\langle O\rangle_\xi$) averages:

$$\langle O\rangle = \frac{\langle Z^{-1/2}O\rangle_\xi}{\langle Z^{-1/2}\rangle_\xi} \tag{14}$$

with Z being the inverse mass metric tensor, defined as

$$Z = \sum_{i=1}^{N}\frac{1}{m_i}\sum_{\mu=x,y,z}\left(\frac{\partial\xi}{\partial x_{i,\mu}}\right)^2 \tag{15}$$

where m_i is the mass of atom i and μ is the component of the Cartesian position vector $\boldsymbol{x}$. The terms $P_i(\xi')$ can easily be obtained from the histogram approximation in a straightforward MD simulation. Equation 12 represents a very appealing alternative to eq 2, since it allows us to "lock", by a suitable choice of the constraint, slow degrees of freedom, such as the hindered translations or rotations, that cause large and slowly fluctuating changes in $V_1 - V_0$.

Using eq 13 entails introducing constrained harmonic force fields (eqs 7 and 8), defined by a modified Hessian matrix $\underline{\bar{\boldsymbol{H}}}^{\boldsymbol{x}}$, which is obtained for a stationary point on the subspace spanned by all coordinates orthogonal to the constraints (as determined in a constrained relaxation), and in which the constrained degree of freedom is projected out via[65−68]

$$\underline{\bar{\boldsymbol{H}}}^{\boldsymbol{x}} = \underline{\bar{\boldsymbol{B}}}_{\boldsymbol{x}_0}^{\mathrm{T}}\underline{\bar{\boldsymbol{A}}}_{\boldsymbol{x}_0}^{\mathrm{T}}\underline{\boldsymbol{H}}^{\boldsymbol{x}}\underline{\bar{\boldsymbol{A}}}_{\boldsymbol{x}_0}\underline{\bar{\boldsymbol{B}}}_{\boldsymbol{x}_0} \tag{16}$$

The projection requires the use of a modified Wilson B-matrix $\underline{\boldsymbol{B}}$ (and its Moore–Penrose pseudo-inverse $\underline{\boldsymbol{A}}$), where all vectors $\underline{\boldsymbol{B}}_j$ were Gram–Schmidt orthogonalized with respect to the vector $\underline{\boldsymbol{B}}_c$, corresponding to the constrained coordinate:

$$\underline{\bar{\boldsymbol{B}}}_j = \underline{\boldsymbol{B}}_j - \frac{(\underline{\boldsymbol{B}}_j \cdot \underline{\boldsymbol{B}}_c)}{|\underline{\boldsymbol{B}}_c|} \frac{\underline{\boldsymbol{B}}_c}{|\underline{\boldsymbol{B}}_c|} \tag{17}$$

The modified Hessian matrix $\underline{\bar{\boldsymbol{H}}}^{\boldsymbol{x}}$ is also used to determine $A_{0,\boldsymbol{x}}(\xi')$ via eq 3, which when combined with eq 13 defines the free energy of the fully interacting constrained system:

$$A_1(\xi') = A_{0,\boldsymbol{x}}(\xi') + \Delta A_{0,\boldsymbol{x}\to 0,\boldsymbol{q}}(\xi') + \Delta A_{0,\boldsymbol{q}\to 1}(\xi') \tag{18}$$

Compared to $\underline{\boldsymbol{H}}^{\boldsymbol{x}}$, the number of non-zero eigenvalues (i.e., the number of vibrational degrees of freedom of the system) of $\underline{\bar{\boldsymbol{H}}}^{\boldsymbol{x}}$ is lowered by the number of independent constraints (see Figure 1).

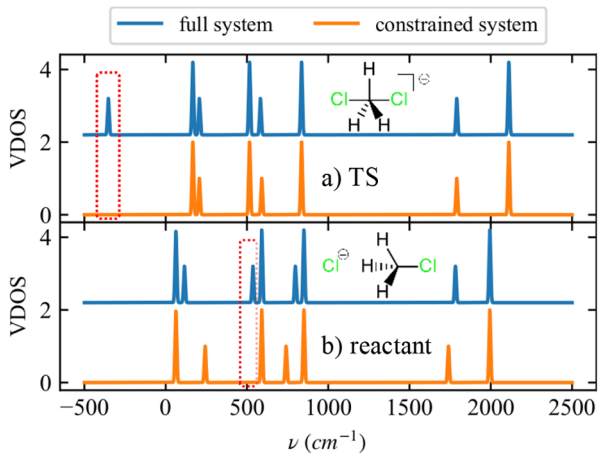

Figure 1. Harmonic vibrational density of states (VDOS) for reactant and transition states of the substitution reaction of CH_3Cl with a Cl^- anion (see more in Section 3.2). Upon projecting out the components corresponding to the constraint (reaction coordinate ξ) from the Hessian matrix, the number of vibrational degrees of freedom is reduced by one. Selecting the constrained coordinate to represent the reaction coordinate, the imaginary frequency (shown as negative frequency) is eliminated in the case of the TS, while the remaining part of the VDOS remains essentially unchanged, indicating that, in this case, ξ is a pure eigenmode of the TS parallel with the imaginary mode.

2.3. Calculation of Activation Free Energy. In transition-state theory, which we employ in this work, the free energy of activation $\Delta A^{\ddagger}_{\mathrm{R}\to\mathrm{P}}$ is determined by[69]

$$\Delta A^{\ddagger}_{\mathrm{R}\to\mathrm{P}} = \Delta A_{\xi_{\mathrm{ref,R}}\to\xi^*} - k_{\mathrm{B}}T \ln\left(\frac{h}{k_{\mathrm{B}}T}\frac{\langle|\dot{\xi}^*|\rangle}{2}P(\xi_{\mathrm{ref,R}})\right) \tag{19}$$

The values $\xi_{\mathrm{ref,R}}$ and ξ^* of the reaction coordinate $\xi(\boldsymbol{x})$ correspond to (an arbitrarily chosen) reactant reference state and the TS on the free energy landscape, respectively. The term $\langle\cdots\rangle$ stands for the NVT ensemble average of the enclosed quantity. The calculation of the last term on the right-hand side of eq 19, for brevity hereinafter labeled $\Delta A_{\mathrm{free_R}\to\xi_{\mathrm{ref,R}}}$, is straightforward.[69] The probability density of the reactant reference state, $P(\xi_{\mathrm{ref,R}}) = \langle\delta(\xi(\boldsymbol{x}) - \xi_{\mathrm{ref,R}})\rangle$, is obtained from an unconstrained MD simulation of the reactant, while the generalized TS velocity $\langle|\dot{\xi}^*|\rangle$ is computed from

$$\langle|\dot{\xi}^*|\rangle = \frac{1}{\langle Z^{-1/2}\rangle_{\xi^*}}\sqrt{\frac{2k_{\mathrm{B}}T}{\pi}} \tag{20}$$

where the inverse mass metric tensor Z (eq 15) comes from a constrained MD simulation for the TS.[47]

The two TI methods discussed in this work differ in the way the term $\Delta A_{\xi_{\mathrm{ref,R}}\to\xi^*}$—interpreted as reversible work needed to shift the value of $\xi(\boldsymbol{x})$ from $\xi_{\mathrm{ref,R}}$ to ξ^*—is determined. In the well-established ξ-TI method, used in this work as benchmark, $\Delta A_{\xi_{\mathrm{ref,R}}\to\xi^*}$ is determined from the integral of free energy gradients along the reaction path ξ connecting the initial and final states:

$$\Delta A_{\xi_{\mathrm{ref,R}}\to\xi^*} = \int_{\xi_{\mathrm{ref,R}}}^{\xi^*}\left(\frac{\partial A}{\partial \xi}\right)_{\xi'} \mathrm{d}\xi' \tag{21}$$

The free energy gradients needed in eq 21 are determined[47,48,70] by

$$\left(\frac{\partial A}{\partial \xi}\right)_{\xi'} = \frac{1}{\langle Z^{-1/2}\rangle_{\xi'}}\left\langle Z^{-1/2}\left[-\lambda + \frac{k_{\mathrm{B}}T}{Z}\sum_{i=1}^{N}\sum_{\mu=x,y,z}\frac{1}{m_i}\frac{\partial \xi}{\partial r_{i,\mu}}\frac{\partial Z}{\partial r_{\mu,i}}\right]\right\rangle \tag{22}$$

using constrained MD simulations with a fixed value of ξ, where λ is the Lagrange multiplier associated with the constraint $\xi(\boldsymbol{x}) = \xi'$ that is used in the SHAKE algorithm.[64] Consequently, the calculation of the free energy difference via ξ-TI requires performing multiple constrained MD simulations not only for the initial and final states but also for several states with intermediate values of ξ. Some of these intermediate states are likely to include structures with large atomic forces, often resulting in uncontrolled escapes from the desired mechanistic routes to undesired alternative reaction channels, ruining thus sampling. In practice, the latter can be avoided by using suitably chosen bias potentials[50,71,72] which, however, often require multiple time-consuming trial–error iterations. Also, the presence of bias potentials always affects the sampling of configuration space and ultimately the free energy calculations, which is rarely accounted for in practice. Furthermore, ξ-TI exhibits an unfavorable propagation of the statistical error which accumulates along the path. Therefore, when one considers a sequence of multiple elementary reactions, the statistical uncertainty in free energy of intermediates increases with their distance from the initial reactant state.[72] Another downside of ξ-TI is that the anharmonicity of the reference system cannot be calculated independently, making a reference to states in the gas phase (e.g., as preferable in heterogeneous catalysis) difficult to impossible.

In this work we propose to determine the term $\Delta A_{\xi_{\mathrm{ref,R}}\to\xi^*}$ using the constrained λ-TI method detailed in Section 2.3. In particular, we employ

$$\Delta A_{\xi_{\mathrm{ref,R}}\to\xi^*} = A_1(\xi^*) - A_1(\xi_{\mathrm{ref,R}}) \tag{23}$$

Table 1. Comparison of Contributions to the Free Energy A_1 of Constrained Reactant Reference ($\xi_{ref,R}$) and Transition (ξ^*) States Obtained Using λ-TI with the Result of the Classical Harmonic Approximation A_{HA}[a]

System	$A_{0,x}$	$\Delta A_{0,x\to 0,q}$	$\Delta A_{0,q\to 1}$	A_1	A_{HA}
ethane ($\xi_{ref,R}$)	−40.6534	−0.0004 ± 0.0000	−0.0013 ± 0.0001	−40.6550 ± 0.0001	−40.6534
ethane (ξ^*)	−40.5399	−0.0003 ± 0.0000	−0.0010 ± 0.0001	−40.5412 ± 0.0001	−40.5399
$CH_3Cl + Cl^-$ ($\xi_{ref,R}$)	−29.4664	−0.0016 ± 0.0001	−0.1611 ± 0.0047	−29.6290 ± 0.0048	−29.6119
$CH_3Cl + Cl^-$ (ξ^*)	−29.1312	−0.0018 ± 0.0001	−0.0173 ± 0.0014	−29.1502 ± 0.0015	−29.1574
rDA ($\xi_{ref,R}$) (I)	−90.3863	−0.0008 ± 0.0000	−0.2617 ± 0.0004	−90.6488 ± 0.0004	−90.4908
rDA ($\xi_{ref,R}$) (II)	−90.6087	−0.0006 ± 0.0000	−0.0498 ± 0.0001	−90.6591 ± 0.0001	−90.6514
rDA (ξ^*)	−88.2174	−0.0009 ± 0.0000	−0.0868 ± 0.0019	−88.3050 ± 0.0019	−88.2623
H^+ transfer ($\xi_{ref,R}$)	−288.4140	−0.0154 ± 0.0005	−0.5555 ± 0.0086	−288.9849 ± 0.0091	−288.9085
H^+ transfer (ξ^*)	−287.7650	−0.0140 ± 0.0005	−0.5265 ± 0.0084	−288.3055 ± 0.0089	−288.2336

[a] $A_{0,x}$, $\Delta A_{0,x\to 0,q}$, and $\Delta A_{0,q\to 1}$ stand for free energy of harmonic reference state, difference in free energy between the system harmonic in internal and Cartesian coordinates, and the free energy difference between anharmonic system and that harmonic in internal coordinates (cf. Section 2.1). The rotational and translational contributions are included in terms $A_{0,x}$, A_1 and A_{HA} via rigid rotor and ideal gas approximations, respectively. In the case of the retro-Diels–Alder (rDA) reaction, results obtained using the half-boat (I) and half-chair (II) reactant reference states are presented. All values are in eV.

where the terms $A_1(\xi_{ref,R})$ and $A_1(\xi^*)$ are the anharmonic free energies of the reactant reference state and TS with $\xi(\boldsymbol{x})$ fixed at $\xi_{ref,R}$ and ξ^*, respectively, which are determined using eq 18.

The advantage of eq 23 over eq 21 lies in fact that it avoids explicit sampling of intermediate states between the reactant state and TS. Since the reactant state and TS are both stationary on the free energy surface, their free energy gradients vanish, remedying thus the problem of uncontrolled escapes mentioned above. Furthermore, as we show in Section 4, the number of integration points used in A_1 calculations of each state can be significantly reduced (in optimal cases only two points are needed). In favorable cases (especially reactions involving low entropy in the reactant state and TS) this λ-TI strategy may thus offer an improved computational efficiency compared to the ξ-TI method. Finally, λ-TI naturally allows for a more detailed analysis of the anharmonic contributions to the free energy barrier, as it can distinguish the contributions from the reactant state and TS.

In the harmonic approximation, eq 19 reduces to

$$\Delta A^{\ddagger}_{R\to P} = A_{HA}(\xi^*) - A_{HA}(\xi_{free,R}) \tag{24}$$

where the harmonic free energies for the TS ($A_{HA}(\xi^*)$) and for the unconstrained reactant ($A_{HA}(\xi_{free,R})$) are computed according to eq 3 using the unmodified Hessian matrix.

Additionally, reactant and transition states of molecular systems contribute their difference in rotational and translational parts to $\Delta A^{\ddagger}_{R\to P}$. In this work, we apply the rigid rotor and ideal gas models[61] to relaxed reactant and transition structures.

2.4. Simulation Details. Periodic DFT calculations were performed using the VASP code.[73−76] The Kohn–Sham equations were solved variationally in a plane-wave basis set using the PAW method of Blöchl, as adapted by Kresse and Joubert with standard PAW potentials.[77,78] The PBE[79] density functional with D2 dispersion correction of Grimme[80] (PBE-D2) as implemented in VASP[81] was applied using a plane wave energy cutoff of 400 eV for all computations. The Brillouin-zone sampling was restricted to the Γ-point.[82] Convergence criteria of 10^{-7} eV and 0.005 eV·Å^{-1} were applied to SCF cycles and geometry optimizations, respectively. The same electronic structure-related setting was used in geometry relaxations and MD simulations. Constrained geometry relaxations were performed using the program GADGET[67,68] and automated relaxed potential energy surface scans.[83] A path passing through a single potential energy barrier connecting reactant state with TS was ensured using the following optimization strategy. First, the transition structure was identified. Subsequently, the system was relaxed along the intrinsic reaction coordinate (IRC) according to the algorithm of Hratchian and Schlegel.[84] Finally, the minimum along the IRC, corresponding to the reactant state, was relaxed using the same convergence criterion as for the TS. A vibrational analysis was performed for the reactant state and TS using the finite differences method with a numerical step of 0.01 Å. The eigenspectra of the dynamical matrices were carefully checked for the correct number of real and imaginary frequencies. From the latter calculations, full Hessian matrices were obtained and used in the λ-TI calculations.

The ξ-TI and λ-TI methods were carried out with MD at the PBE-D2 level of theory in the NVT ensemble as implemented[53,85] in VASP 6.3. The simulation temperature was maintained using the Andersen thermostat with a collision probability of 0.05.[86] Similar to previous studies,[53,87] hydrogen atoms were treated as tritium (mass = 3 u) because this allows one to use a larger time step when integrating the equations of motion. Consistently, the mass of tritium was also used for the computation of all harmonic frequencies. Equilibration periods in MD were determined with the Mann–Kendall test for trends in mean and variance.[88] Thermodynamic integrations were performed numerically using the Simpson integration scheme adapted to irregularly spaced grid points.[89−91] The standard integration grid used in the λ-TI calculations consisted of five points ($\lambda \in \{0.00, 0.25, 0.50, 0.75, 1.00\}$). In explicitly mentioned specific cases, this set was extended by additional points. The choice of the reaction coordinate for the $\Delta A^{\ddagger}_{R\to P}$ calculations and the choice of the integration grid for the ξ-TI method are discussed for each system separately, see Section 3. The sets of redundant internal coordinates (distances, angles, dihedrals) in our λ-TI simulations were generated automatically from neighborship relations with cutoff distances based on scaled atomic covalent radii.[53] The statistical error was determined as described in Section S1 of the Supporting Information.

3. RESULTS AND DISCUSSION

We benchmark free energy barriers computed using our λ-TI method against the ξ-TI method for a selection of reactions, including the unimolecular rotamerization of ethane, the

degenerate second-order nucleophilic substitution of CH_3Cl by a Cl^- anion, the retro-Diels–Alder prototype reaction, and a proton transfer in acidic chabazite (zeolite H-SSZ-13). Tabular summaries of the results are provided in Tables 1–4. In particular, all free energy contributions from λ-TI are shown in Table 1, along with the corresponding results in the harmonic approximation. The free energy differences $\Delta A_{\xi_{\mathrm{ref,R}} \to \xi^*}$ between the constrained reactant state and TS computed by ξ-TI, λ-TI, and HA are compared in Table 2. The results for the term

Table 2. Free Energy Differences $\Delta A_{\xi_{\mathrm{ref,R}} \to \xi^*}$ between the Constrained Reactant State and TS Computed by ξ-TI and λ-TI Compared to the Corresponding Harmonic Approximation ΔA_{HA}[a]

Reaction	T/K	ξ-TI/meV	λ-TI/meV	HA/meV
ethane rotation	400	117.4 ± 4.9	113.8 ± 0.1	113.5
$CH_3Cl + Cl^-$	600	472.9 ± 3.7	478.8 ± 6.3	454.5
rDA (I)	400	2336.5 ± 6.9	2343.8 ± 0.5	2228.5
rDA (II)	400	2328.8 ± 7.1	2354.1 ± 0.2	2389.1
H^+ transfer	600	672.3 ± 11.1	679.4 ± 18.0	674.9

[a]The rotational and translational contributions to reactant reference and transition states are included via rigid rotor and ideal gas approximations, respectively. In the case of the retro-Diels–Alder (rDA) reaction, results obtained using the half-boat (I) and half-chair (II) reactant reference states are presented.

$\Delta A_{\mathrm{free_R} \to \xi_{\mathrm{ref,R}}}$ that connects the constrained and free reactant states are shown in Table 3. The final ξ-TI, λ-TI, and HA values of $\Delta A^{\ddagger}_{\mathrm{R} \to \mathrm{P}}$ are compared in Table 4.

3.1. Internal Rotation of Ethane. The first reaction selected to benchmark λ-TI against ξ-TI is the rotamerization of ethane at 400 K. For this transformation, the reaction coordinate can be chosen as a symmetric linear combination of three dihedral angles $\left(\xi = \frac{1}{3}(\tau_1 + \tau_2 + \tau_3)\right)$, schematically shown in Figure 2. For the relaxed staggered reactant state and ecliptic TS, the values of ξ are 1.048 rad and 0.000 rad, respectively, the latter value being fixed by symmetry. Naturally, the relaxed reactant was chosen as the reactant reference state in our ξ-TI and λ-TI calculations.

The lengths of trajectories generated by free DFT MD, by constrained DFT MD, and by constrained harmonic force field MD simulations were 100 ps, 25 ps, and 50 ps, respectively. A time step of 0.5 fs was used in the MD simulations. The ξ-TI calculations were performed using seven grid points (black markers in Figure 2) distributed between reactant reference configuration and TS.

Table 4. Free Energy Barriers $\Delta A^{\ddagger}_{\mathrm{R} \to \mathrm{P}}$ Computed by the ξ-TI and λ-TI Methods Compared to the Corresponding HA Results[a]

Reaction	T/K	ξ-TI/meV	λ-TI/meV	HA/meV
ethane rotation	400	138.9 ± 4.9	135.0 ± 0.1	130.2
$CH_3Cl + Cl^-$	600	531.1 ± 3.7	537.0 ± 6.3	474.2
rDA (I)	400	2280.6 ± 6.9	2287.9 ± 0.5	2193.2
rDA (II)	400	2259.0 ± 7.1	2284.3 ± 0.2	2354.7
H^+ transfer	600	665.3 ± 11.1	672.4 ± 18.0	693.8

[a]The rotational and translational contributions to reactant reference and transition states are included via rigid rotor and ideal gas approximations, respectively. In the case of the retro-Diels–Alder (rDA) reaction, results obtained using the half-boat (I) and half-chair (II) reactant reference states are presented.

The computed values of $\Delta A^{\ddagger}_{\mathrm{R} \to \mathrm{P}}$ obtained in ξ-TI and λ-TI are 138.9 ± 4.9 meV and 135.0 ± 0.1 meV, respectively. Therefore, both methods yield nearly perfectly consistent predictions for this quantity. A comparison with the result of the HA (130.2 meV) reveals that anharmonicity leaves the free energy barrier of the internal rotation of ethane almost unchanged. Further comparison of A_1 and A_{HA} in Table 1 shows that anharmonicity is negligible for both the constrained reactant reference state and the TS. The free reactant state is therefore the largest, albeit still small, contributor of anharmonicity to $\Delta A^{\ddagger}_{\mathrm{R} \to \mathrm{P}}$.

3.2. Nucleophilic Substitution of CH_3Cl. The second benchmark is performed on the nucleophilic substitution of CH_3Cl with a Cl^- anion at 600 K. Its reaction coordinate can be approximated by the difference between the interatomic distances d_1 and d_2 involved in the formation and cleavage of bonds ($\xi = d_2 - d_1$), see Figure 3. The relaxed reactant state is a van der Waals complex where Cl^- weakly interacts with neutral CH_3Cl at ξ = 1.269 Å, while the product is a symmetry-equivalent state with ξ = −1.269 Å. The TS is symmetric, whereby both C–Cl bonds are broken and ξ is fixed at 0.000 Å (Figure 3). The HA yields a free energy barrier of 442.3 meV.

In the MD simulations presented here, a time step of 1.0 fs was used. The trajectory lengths were 200 ps for the free DFT MD simulation determining $P(\xi)$, 80 ps per constrained DFT MD simulation performed within the ξ-TI and λ-TI methods, and 50 ps per harmonic force field MD simulation contributing to $A_{0,\boldsymbol{x} \to 0,\boldsymbol{q}}$. Using the ξ-TI method, constrained MD runs were performed for eight states (black markers in Figure 3) distributed on the interval between the reactant reference state and the TS (see Figure 3). The standard λ-TI grid defined in Section 2.4 was extended by two extra points (λ = 0.90 and 0.95) for the DFT MD simulations of the reactant reference state. The denser grid was needed to account for a

Table 3. Data for the Calculation of $\Delta A_{\mathrm{free_R} \to \xi_{\mathrm{ref,R}}}$[a]

Reaction	T/K	$\xi_{\mathrm{ref,R}}$	$\langle \lvert \dot{\xi}^* \rvert \rangle$	$P(\xi_{\mathrm{ref,R}})$	$\Delta A_{\mathrm{free_R} \to \xi_{\mathrm{ref,R}}}$/meV
ethane rotation	400	1.048 rad	6.739×10^{12} rad s^{-1}	1.323 rad^{-1}	21.6
$CH_3Cl + Cl^-$	600	1.269 Å	1.106×10^{13} Å s^{-1}	0.733 $Å^{-1}$	58.2
rDA (I)	400	0.049	1.745×10^{12}	48.288	−55.9
rDA (II)	400	0.042	1.745×10^{12}	72.429	−69.8
H^+ transfer	600	−1.660 Å	1.989×10^{13} Å s^{-1}	1.438 $Å^{-1}$	−7.0

[a]See Section 2.3. In the case of the retro-Diels–Alder (rDA) reaction, results obtained using the half-boat (I) and half-chair (II) reactant reference states are presented.

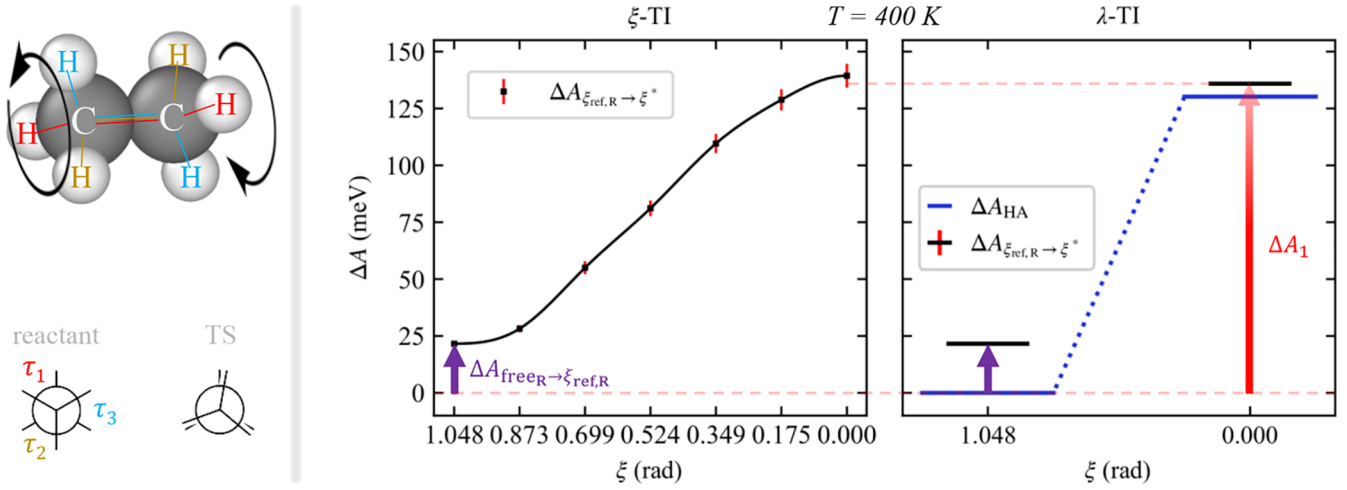

Figure 2. Reaction coordinate (ξ) for the rotamerization of ethane is described by the symmetric linear combination of dihedral angles τ_1, τ_2, and τ_3 (left). The free energy barriers obtained by ξ-TI (middle) and λ-TI (right) at 400 K are compared with the harmonic approximation result ΔA_{HA} (blue). The error bar in λ-TI is below the resolution.

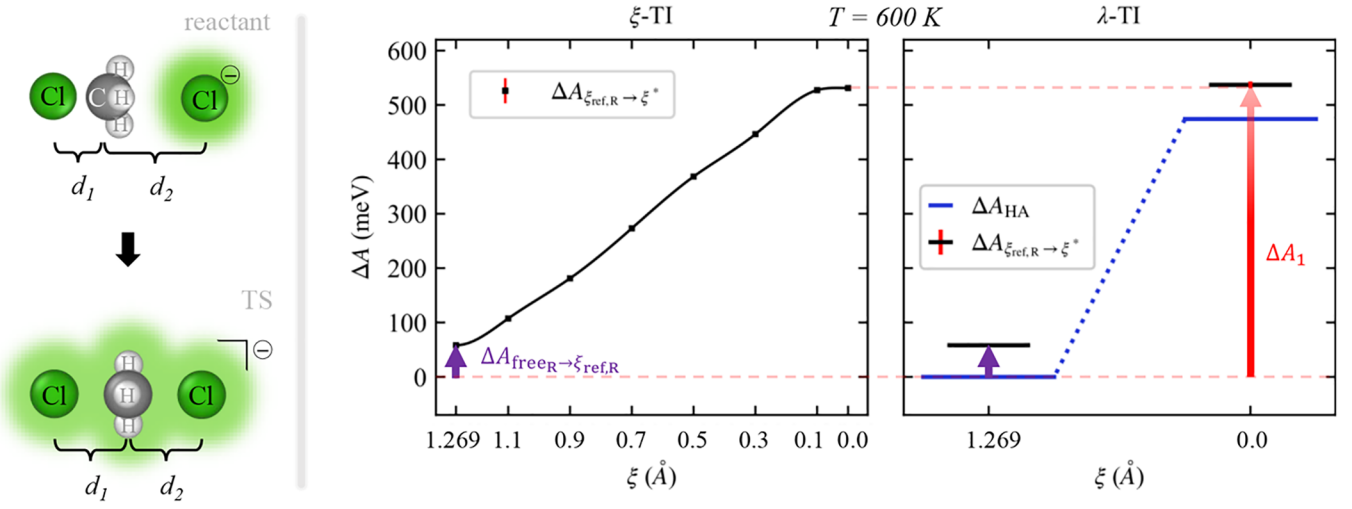

Figure 3. Reaction coordinate (ξ) for the nucleophilic substitution of CH_3Cl with Cl^- described by an antisymmetric linear combination of the interatomic distances d_1 and d_2 (left). The free energy barriers obtained by ξ-TI (middle) and λ-TI (right) at 600 K are compared with the harmonic approximation result ΔA_{HA} (blue).

rapid decrease of the integrand in eq 13 near the upper integration limit.

The ξ-TI method yields $\Delta A_{\xi_{ref,R}\to\xi^*}$ = 472.0 ± 3.7 meV, while the λ-TI method determines the same quantity as 478.8 ± 6.3 meV. The two methods are therefore in very good agreement. Comparing these results with the value of 454.5 meV resulting from the constrained HA suggests that the anharmonic contribution to $\Delta A_{\xi_{ref,R}\to\xi^*}$ is only modest, which either can be a consequence of low anharmonicities of both the reactant reference state and the TS or may result from a cancellation of two anharmonic contributions of similar magnitude. The former cause is confirmed when comparing A_1 and A_{HA} in Table 1—we find that the anharmonic corrections are −17.1 eV and 7.2 meV for the constrained reactant reference state and TS, respectively, thereby increasing the free energy barrier by 24.3 meV.

Accounting for the term $A_{free_R\to\xi_{ref,R}}$ = 58.2 meV yields a $\Delta A^{\ddagger}_{R\to P}$ of 531.1 meV obtained by ξ-TI and of 537.0 meV obtained by λ-TI. As evident from the comparison with the HA (474.2 meV), the term $\Delta A_{free_R\to\xi_{ref,R}}$ adds another ∼40 meV to the anharmonic correction of the barrier. This result can be understood intuitively. As shown in Figure 4, anharmonicity shifts the maximum of $P(\xi)$ toward larger values, which is directly caused by the thermal destabilization of the nonbonding C−Cl interaction. Thus, $P(\xi_{ref,R})$ decreases from the harmonic probability density $P_{0,x}(\xi_{ref,R})$ of 1.517 $Å^{-1}$ to the anharmonic one $P_1(\xi_{ref,R})$ of 0.733 $Å^{-1}$, and this change is linked with the change in free energy (see eq 19) of $-k_BT\ln(P_1(\xi_{ref,R})/P_{0,x}(\xi_{ref,R}))$ = 37.6 meV. The latter value is virtually identical to the anharmonic contribution of $\Delta A_{free_R\to\xi_{ref,R}}$ reported above.

3.3. Retro-Diels−Alder Reaction. In this section we discuss the calculation of the free energy barrier for the retro-Diels−Alder (rDA) reaction of cyclohexene to ethene and butadiene at 400 K. In the relaxed transition structure, depicted in Figure 5, ethene is already clearly detached from butadiene, with the shortest intermolecular C−C separations being >2.3

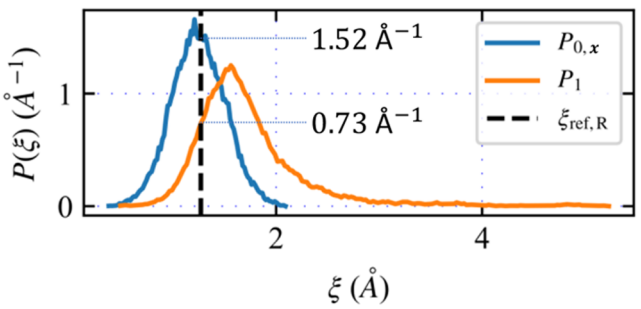

Figure 4. Probability distribution of ξ for the unconstrained reactant state chosen for the substitution reaction of CH_3Cl with Cl^-. The results obtained by considering the harmonic approximation ($P_{0,x}$) and a full anharmonic interaction (P_1) are compared. The dashed line marks the position of the reactant reference state.

Å. The reactant structure obtained by descending from the transition structure along the IRC path and a subsequent relaxation corresponds to a half-boat conformer of cyclohexene (see Figure 6). The free energy barrier computed in the HA amounts to 2193.2 meV.

The reaction coordinate ξ for the rDA reaction was represented by the path-based variable according to Branduardi et al.:[92]

$$\xi(\boldsymbol{x}) = \frac{1}{M-1}\frac{\sum_{i=1}^{M}(i-1)\exp(-\lambda|\chi(\boldsymbol{x})-\tilde{\chi}_i|^2)}{\sum_{i=1}^{M}\exp(-\lambda|\chi(\boldsymbol{x})-\tilde{\chi}_i|^2)} \quad (25)$$

where $\chi(\boldsymbol{x})$ is a four-dimensional vector, with the components being the interatomic distances d_1 to d_4 shown in Figure 5. The IRC was discretized using $M = 7$ reference structures with the Cartesian coordinates $\tilde{\boldsymbol{x}}_i$ and the internal coordinates $\tilde{\chi}_i = \chi(\tilde{\boldsymbol{x}}_i)$ that form the basis to express ξ. The expression $|\cdots|$ represents the Euclidean norm of the vector enclosed. The parameter λ was set to 1.88 Å^{-2}, which corresponds to the average of the inverse of the mean-square displacement between successive frames, as proposed by Branduardi et al.[92]

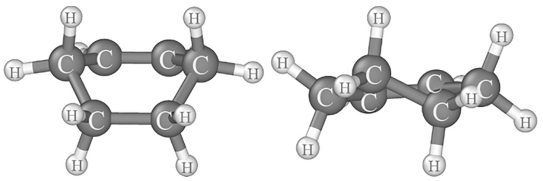

Figure 6. Half-boat (left) and the more stable half-chair (right) conformations of cyclohexene that were used as reactant reference states for the retro-Diels–Alder reaction.

The length of the constrained DFT MD simulations was set to 50 ps, while a trajectory of 100 ps was produced in the free MD run to determine $P(\xi)$. The length of the MD trajectories in the harmonic force field MD simulations for the λ-TI method was 50 ps. Time steps of 1 fs and 0.5 fs were used in the DFT and the harmonic force field MD simulations, respectively. The ξ-TI calculations were performed with the grid of eight points shown as black markers in Figure 5. The lowest value of this integration grid (0.049) corresponds to ξ determined for the relaxed reactant that we chose as the reactant reference state. Unlike in the two previous reactions discussed above, the value of ξ in the TS is not fixed by symmetry. To ensure that the finite-temperature TS falls into the interval of sampled ξ, we chose the largest value of the integration grid to be slightly larger than ξ determined for the relaxed TS (0.287). According to our ξ-TI calculations, however, the position of the TS (ξ = 0.283, identified as the point with vanishing free energy gradient) barely changes at the temperature considered here (see Figure 5). The DFT MD simulations for the reactant reference state were carried out with two additional grid points (λ = 0.90 and 0.95) to account for a rapid decrease of the integrand in eq 13 near the upper integration limit.

The ξ-TI and λ-TI results are presented in Figure 5. As evident, the two methods yield almost identical values of $\Delta A^{\ddagger}_{\mathrm{R}\to\mathrm{P}}$ (2280.6 ± 6.9 meV and 2287.9 ± 0.5 meV, respectively), which are, however, ~90 meV higher compared to the HA result. Virtually the same difference between HA

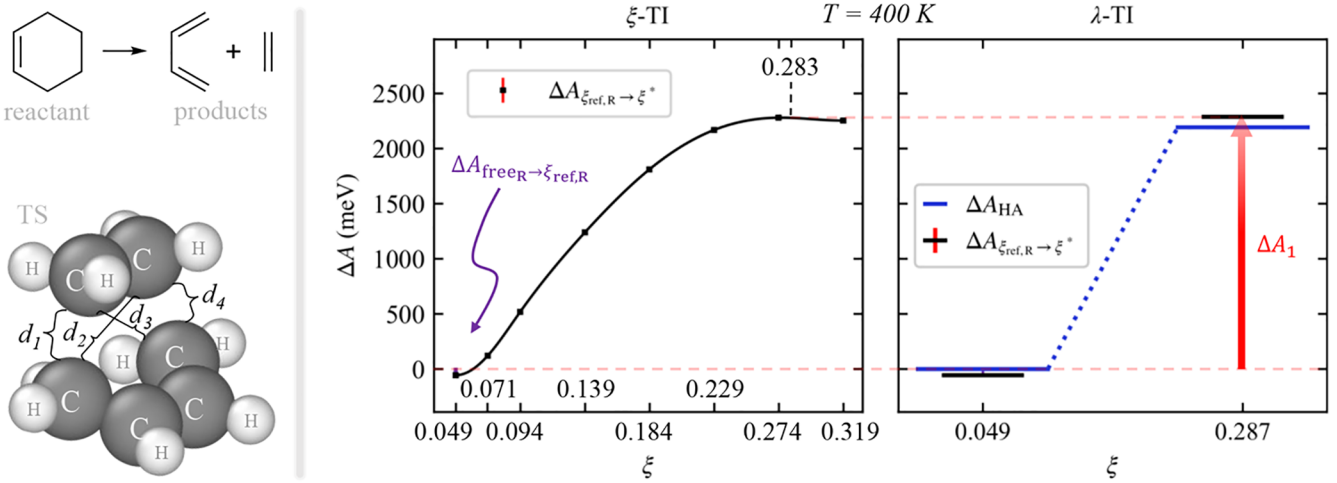

Figure 5. Reaction coordinate (ξ) for the retro-Diels–Alder reaction of cyclohexene to ethene and butadiene described by path-based variables involving the interatomic distances d_1 to d_4 (left). Free energy barriers obtained by ξ-TI (middle) and λ-TI (right) at 400 K are compared with the harmonic approximation result ΔA_{HA} (blue). The half-boat conformer was considered as the reactant reference state. The error bars are below the resolution.

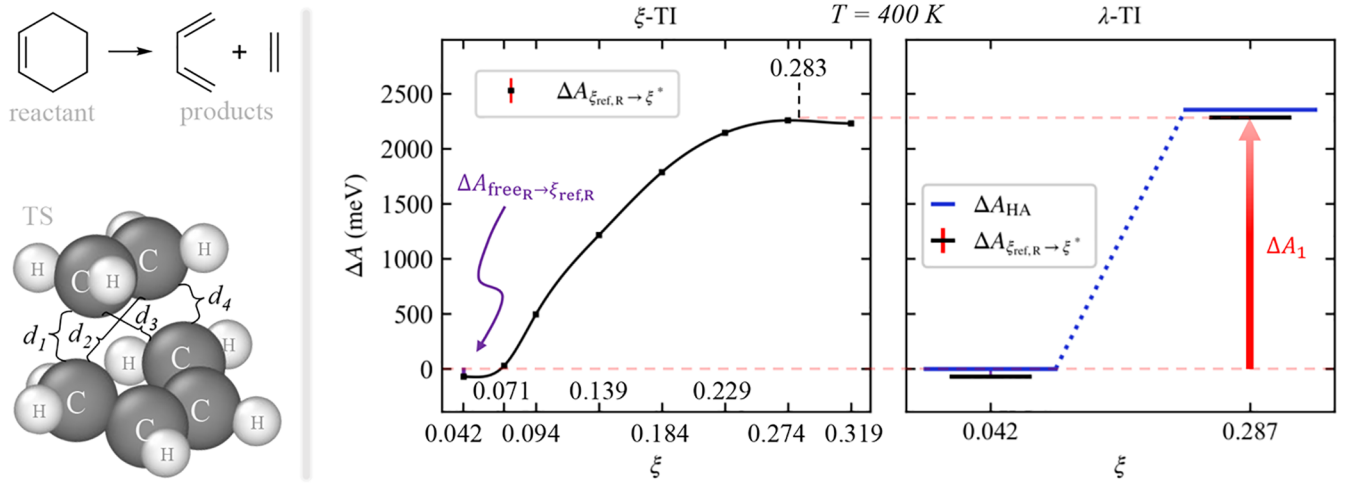

Figure 7. Reaction coordinate (ξ) for the retro-Diels–Alder (rDA) reaction of cyclohexene to ethene and butadiene, described by a path-based variable involving the interatomic distances d_1 to d_4 (left). Free energy barriers obtained by ξ-TI (middle) and λ-TI (right) at 400 K compared with the harmonic approximation result ΔA_{HA} (blue). The half-chair conformer was considered as the reactant reference state. The error bars are below the resolution.

and the TI methods is present already in the term $\Delta A_{\xi_{ref,R}\to\xi^*}$ (see Table 2). Once again, our λ-TI is useful in interpreting the origin of this difference. From the comparison of A_1 and A_{HA} in Table 1, it follows that the anharmonic contribution to the free energy of the reactant reference state is much larger in absolute value than that for the TS (−158.0 meV vs −42.7 meV). A visual inspection reveals that the half-boat conformer of the reactant reference state (cyclohexene), obtained by relaxing along the IRC, is unstable in the MD runs and converts into the half-chair conformer (see Figure 6). Upon relaxation of the latter, it is clear that the half-chair conformer is 161.5 meV lower in A_{HA} than the half-boat conformer. Choosing this more stable alternative as the reactant reference state leads to a repartitioning of the $A_{\text{free}_R\to\xi_{ref,R}}$ and $\Delta A_{\xi_{ref,R}\to\xi^*}$ contributions to $\Delta A^{\ddagger}_{R\to P}$ (cf. Figures 5, 7 and 8), while the HA now yields a

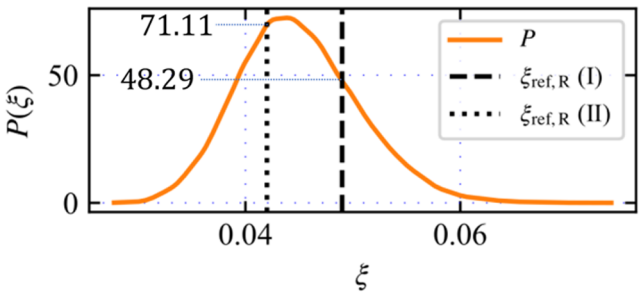

Figure 8. Probability distribution of the unconstrained reactant state for the rDA reaction. The dashed and dotted lines mark the positions of the half-boat (ξ = 0.0489) and half-chair (ξ = 0.0423) reactant reference states, respectively.

free energy barrier of 2354.7 meV. Importantly, however, the ξ-TI and λ-TI results for $\Delta A^{\ddagger}_{R\to P}$ are independent of the choice of the reactant reference state, and thus the results obtained with the alternative reactant reference state (2259.0 ± 7.1 meV and 2284.3 ± 0.2 meV, respectively) are very similar to the ones reported above (see Figure 7), as it should be. In contrast to the conclusion drawn by considering the half-boat reference in the HA, anharmonicity decreases rather than increases the free energy barrier. Furthermore, the HA obviously does not allow for switching between multiple (meta-)stable states, which should also be perceived as an anharmonic effect. The results presented here show that the presence of multiple metastable states accessible at the simulation temperature is at least as important as other contributions to anharmonicity.

3.4. Proton Transfer in Acidic Chabazite. The final benchmark reaction that we discuss is a proton transfer in zeolite H-SSZ-13 (chabazite) at 600 K. The reactant shown in Figure 9 comes with the H atom attached to a framework O atom, forming a bridging O–H group. In the TS, the O–H bond is being broken, and, simultaneously, another one is being formed. The H atom is thus located approximately midway between two framework O atoms. Similar to the substitution reaction discussed in Section 3.2, the difference between two O–H distances ($\xi = d_2 - d_1$, see Figure 9) is used as approximation to the reaction coordinate. The values of ξ in the relaxed reactant state and TS are −1.660 Å and −0.030 Å, respectively. The relaxed reactant was used as the reactant reference state in the calculations discussed here. The free energy barrier computed in the HA is 693.7 meV.

DFT-based MD production runs of 50 ps were carried out with a time step of 1.0 fs. The term $A_{0,x\to0,q}$ was evaluated on production runs with the same length and time step. The integration grid used for the ξ-TI method consisted of the five points shown in Figure 9, including the relaxed reactant state (ξ = −1.660 Å) and TS (ξ = −0.030 Å). We note that the free energy gradient in the TS nearly vanishes and hence, in accord with a previous report,[93] we conclude that its position does not significantly change due to temperature. In the DFT MD simulations for the λ-TI method, we extended the standard grid by an extra point at λ = 0.95 for both the reactant state and TS.

The values of $\Delta A^{\ddagger}_{R\to P}$ computed using the ξ-TI and λ-TI methods, shown in Figure 9, are very similar (665.3 ± 11.1 meV vs 672.2 ± 18.0 meV). Since these results are only <30 meV lower than the barrier in the HA, it appears that anharmonic effects are unimportant for the proton transfer. However, the comparison of A_1 with A_{HA} in Table 1 shows significant anharmonicity for both the reactant reference state

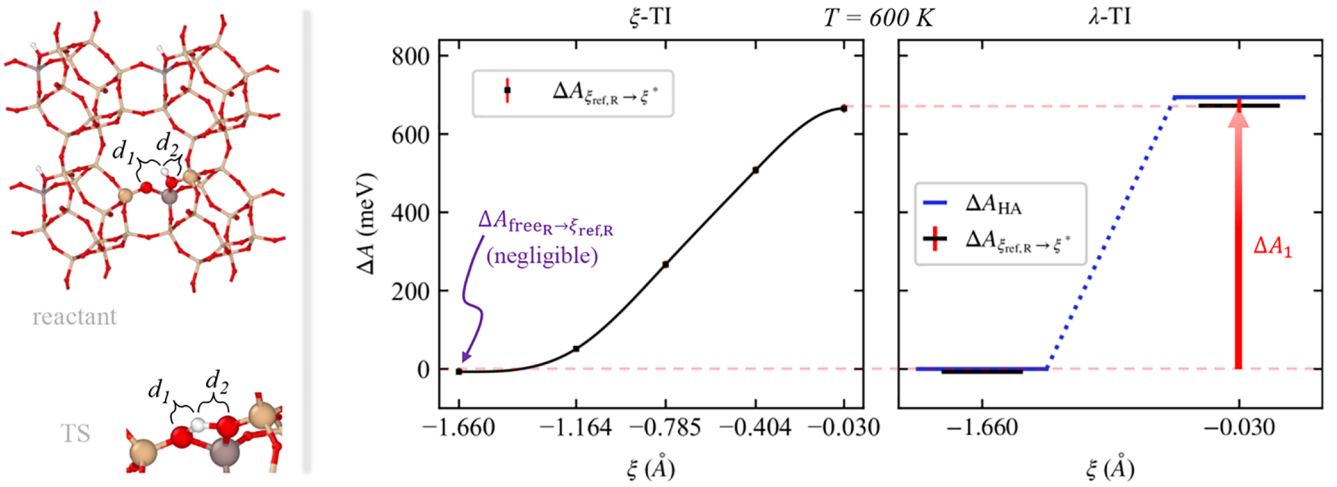

Figure 9. Reaction coordinate (ξ) for a proton transfer in zeolite H-SSZ-13, described by a difference between the interatomic distances d_2 and d_1 (left). Free energy barriers obtained by ξ-TI (middle) and λ-TI (right) at 600 K are compared to the harmonic approximation ΔA_{HA} (blue).

Table 5. Free Energies A_1 (in eV) Obtained from λ-TI via Explicit Numerical Integration (ENI) Using Multiple Integration Points along λ and via the Bennett Acceptance Ratio (BAR) Method Using the Initial (λ = 0) and Final (λ = 1) Grid Points[a]

System	ENI	BAR	I_w
ethane ($\xi_{ref,R}$)	−40.6550 ± 0.0001	−40.6551 ± 0.0004	0.306
ethane (ξ^*)	−40.5412 ± 0.0001	−40.5414 ± 0.0004	0.312
$CH_3Cl + Cl^-$ ($\xi_{ref,R}$)	−29.6290 ± 0.0048	−29.6380 ± 0.0069	0.023
$CH_3Cl + Cl^-$ (ξ^*)	−29.1502 ± 0.0015	−29.1519 ± 0.0019	0.237
rDA ($\xi_{ref,R}$) (I)	−90.6488 ± 0.0004	−90.6392 ± 0.0377	0.020
rDA ($\xi_{ref,R}$) (II)	−90.6591 ± 0.0001	−90.6600 ± 0.0037	0.106
rDA (ξ^*)	−88.3050 ± 0.0019	−88.3043 ± 0.0052	0.054
H^+ transfer ($\xi_{ref,R}$)	−288.9849 ± 0.0091	−288.9667 ± 0.0220	0.001
		(−288.9718 ± 0.0059)	(0.028)
H^+ transfer (ξ^*)	−288.3055 ± 0.0089	−288.3572 ± 0.0255	0.003
		(−288.3047 ± 0.0055)	(0.028)

[a]The index I_w measures the overlap between the configuration spaces sampled by MD driven by harmonic and fully interacting potentials. The rotational and translational contributions to reference reactant and transition states are included via rigid rotor and ideal gas approximations, respectively. For the retro-Diels–Alder (rDA) reaction, the presented results include the half-boat (I) and half-chair (II) reference reactant states. The BAR results for the H^+ transfer were also computed with the additional grid points λ = 0.75 and 0.95, for which the results are shown in parentheses.

and the TS (−76.4 meV and −71.9 meV, respectively) which, however, cancels out due to the opposite signs of their contributions to $\Delta A^{\ddagger}_{R\to P}$.

4. ACCELERATING λ-TI VIA THE BAR METHOD

We have demonstrated that the λ-TI method yields predictions of free energy barriers equivalent to the benchmark ξ-TI method. The use of λ-TI is advantageous in cases where the application of ξ-TI requires sampling of regions with large free energy gradients. Nevertheless, the practical execution of the λ-TI method as presented so far requires relatively dense integration grids for the reactant state and TS, thus being typically not more efficient to compute than the ξ-TI method. Inspired by the work of König et al.,[52] we now borrow ideas from free energy perturbation theory[31] and examine the possibility of evaluating $\Delta A_{0\to1}$ using the Bennett acceptance ratio (BAR) method.[51] Unlike the explicit numerical integration (ENI) over a grid of λ values (which we did up to this point, see Section 3), the BAR method ideally requires sampling for only two grid points (λ = 0.0 and 1.0).

In a nutshell, the BAR alternative for eq 5 is written

$$\Delta A_{\alpha\to\beta} = -k_B T \ln \frac{n_\beta}{n_\alpha} + C \tag{26}$$

where n_α and n_β are the numbers of MD steps performed with $\lambda = \alpha$ and β, respectively, and C is a constant determined iteratively so as to fulfill the condition

$$\left\langle \left(1 + \exp\left[\frac{V_\beta - V_\alpha - C}{k_B T}\right]\right)^{-1} \right\rangle_0 = \left\langle \left(1 + \exp\left[\frac{V_\alpha - V_\beta + C}{k_B T}\right]\right)^{-1} \right\rangle_1 \tag{27}$$

The standard error ($\sigma_{\Delta A}$) in $\Delta A_{\alpha\to\beta}$ can be estimated from[31,51]

$$\sigma^2_{\Delta A} = \frac{1}{N_\alpha \beta^2}\left(\frac{\left\langle \left(1 + \exp\left[\frac{V_\beta - V_\alpha - C}{k_B T}\right]\right)^{-2}\right\rangle_0}{\left\langle \left(1 + \exp\left[\frac{V_\beta - V_\alpha - C}{k_B T}\right]\right)^{-1}\right\rangle_0^2} - 1\right) + \frac{1}{N_\beta \beta^2}\left(\frac{\left\langle \left(1 + \exp\left[\frac{V_\alpha - V_\beta + C}{k_B T}\right]\right)^{-2}\right\rangle_1}{\left\langle \left(1 + \exp\left[\frac{V_\alpha - V_\beta + C}{k_B T}\right]\right)^{-1}\right\rangle_1^2} - 1\right) \quad (28)$$

where N_α and N_β correspond to n_α and n_β corrected for the time correlation between MD-generated structures, which can be achieved, for example, via the blocking method.[94] Note that if holonomic constraints are employed, all thermodynamic averages appearing in eqs 27 and 28 have to be reweighted according to eq 14.

Applying the BAR method, we reevaluated the anharmonic free energies A_1 using only the end points $\lambda = 0$ and 1 of the existing data. In Table 5, the values of A_1 for the stationary states of all reactions discussed in Section 3 computed by the BAR method are summarized and compared to those computed by ENI (determined from the values in Table 1). As evident, both approaches yield very similar results for all reactions but the H^+ transfer, where the deviation is unacceptably large for the TS (>50 meV). Moreover, the statistical uncertainties for the reactant state and TS of the proton transfer are unusually large compared to those for the other states shown in Table 5. The prerequisite for reliable results from the simple two-stage BAR procedure is a good overlap of the configuration spaces sampled by MD corresponding to the action of the Hamiltonians $\mathcal{H}_0$ and $\mathcal{H}_1$.[31,95] The overlap can be measured, e.g., via the I_w index,[93,95] defined so that $0.0 < I_w \leq 0.50$, whereby the lower and upper limit values indicate no overlap and a perfect overlap, respectively. A very poor overlap for both states of the H^+ transfer reaction can be deduced from the values of I_w presented in Table 5, which are at least an order of magnitude smaller than those determined for the states of the other reactions. When failing to fulfill the prerequisite of a good match between the configuration spaces sampled under the action of the harmonic and anharmonic potentials, one can resort to multistage sampling, whereby $\Delta A_{\alpha\to\beta}$ is expressed as

$$\Delta A_{\alpha\to\beta} = \Delta A_{\alpha\to\lambda_1} + \sum_{i=1}^{M-1} \Delta A_{\lambda_i\to\lambda_{i+1}} + \Delta A_{\lambda_M\to\beta} \quad (29)$$

with M being the number of points other than $\lambda = 0$ and 1, and $\Delta A_{\lambda_i\to\lambda_j}$ is computed by a straightforward generalization of eq 26. We applied this multistage procedure to both states of the proton transfer using two extra points, $\lambda_1 = 0.75$ and $\lambda_2 = 0.95$. As shown in Table 5, the quality of overlap improved (I_w values increased from values between 0.001 and 0.003 to 0.028), the discrepancy between the values obtained from BAR and ENI was reduced to 13 meV and also the statistical uncertainty decreased almost by a factor 4.

5. CONCLUSIONS AND OUTLOOK

We presented constrained thermodynamic λ-path integration (λ-TI) as a tool to compute anharmonic corrections to the harmonic approximation (HA) of free energy barriers. Using translationally and rotationally invariant curvilinear coordinates, the utility of the approach was demonstrated on four examples with increasing complexity, ranging from a simple unimolecular reaction to a reaction in an extended system. Excellent agreement of our λ-TI method with respect to the well-established ξ-TI method Carter et al.[47] is reported. In addition, the λ-TI method enables a quantification of the individual anharmonic contributions from reactant and transition states, thus providing further insight into the source of anharmonicity. The rotamerization of ethane with prevailing covalent bonds showed little anharmonicity, which was to be expected from previous analysis of the importance of anharmonic contributions for different interactions and degrees of freedom (dissociation contributes more than hindered rotation; vibrations of covalent bonds contribute the least).[53] Significant anharmonic contributions were observed for the nucleophilic substitution reaction of CH_3Cl with Cl^-, which we attributed to the weakly bound nature of the reactant state. For the retro-Diels–Alder reaction, anharmonic contributions were relatively large, and their major part can be attributed to the temperature-induced change of reactant conformations. The anharmonic correction to the barrier of the proton transfer in zeolite H-SSZ-13 is comparatively small, because the individually significant anharmonic corrections to constrained reactant and transition states largely cancel each other. The largest portion of the small anharmonic correction to the barrier can be attributed to the difference between constrained and free reactant states, where the HA deviates more for the free state. Henceforth, the λ-TI method can be seen as a valuable computational tool to compute and analyze anharmonic contributions to free energy barriers. Besides its use in the quantification of anharmonicity effects for individual states, another advantage of λ-TI over ξ-TI is that it avoids sampling over the whole reaction path connecting reactant with TS. In fact, unwanted side reactions can make the sampling of intermediate states with large free energy gradients along the reaction coordinate very difficult in the ξ-TI method. In reactions with more than one reactant (or product), λ-TI could be applied separately to the isolated reactants (or products), whereas ξ-TI requires sampling of all reactants and products in the same simulation box at all times. This is especially troublesome if one is interested in large reaction networks, as this makes the identification of a relevant reference system difficult. The λ-TI method elegantly circumvents this issue and allows us to calculate the anharmonicity of any point (adsorption energy or TS) along the reaction coordinate. Importantly, this also gives a direct reference to the gas phase, which is difficult to impossible with ξ-TI. We are therefore convinced that this method will be valuable to investigate the effect of anharmonicity in complex reaction networks.

Finally, we showed that the λ-TI method can be computationally much more efficient when combined with the Bennett acceptance ratio (BAR) method, effectively reducing the number of integration points to ideally two per stationary state. We note that the use of the BAR method in connection with calculation of free energy profiles of reactions was proposed also be Li et al.,[96] whereby the ab initio quality results were obtained upon application of free energy perturbation theory to data from umbrella sampling[44] simulations performed at a semi-empirical reference method level. Unlike the λ-TI method proposed in this work, the

approach of Li et al. requires the sampling over multiple states along the reaction path. Further promising ways to accelerate the simulations include on-the-fly machine learning, such as SOAP-GAP in VASP,[97,98] or the tight-binding frameworks, for instance as provided by Bannwarth et al.[99] One such example is the work of Blöndal et al.[100] on machine-learned surrogate potential energy surfaces for the translation of adsorbates. Besides the employed internal coordinates, other continuous, unique, and non-degenerate coordinate descriptors—for instance SOAP[101] or components of Ewald sum (Coulomb) matrices[102]—could be utilized as long as they meet the criterion of invariance with respect to overall rotations and translations of the system.

AUTHOR INFORMATION

Corresponding Authors

Jonas Amsler − *Institute of Catalysis Research and Technology, Karlsruhe Institute of Technology, 76344 Eggenstein-Leopoldshafen, Germany;* orcid.org/0000-0003-3112-4957; Email: jonas.amsler@kit.edu

Tomáš Bučko − *Department of Physical and Theoretical Chemistry, Faculty of Natural Sciences, Comenius University in Bratislava, SK-84215 Bratislava, Slovakia; Institute of Inorganic Chemistry, Slovak Academy of Sciences, SK-84236 Bratislava, Slovakia;* orcid.org/0000-0002-5847-9478; Email: bucko19@uniba.sk

Authors

Philipp N. Plessow − *Institute of Catalysis Research and Technology, Karlsruhe Institute of Technology, 76344 Eggenstein-Leopoldshafen, Germany*

Felix Studt − *Institute of Catalysis Research and Technology, Karlsruhe Institute of Technology, 76344 Eggenstein-Leopoldshafen, Germany; Institute for Chemical Technology and Polymer Chemistry, Karlsruhe Institute of Technology, 76131 Karlsruhe, Germany;* orcid.org/0000-0001-6841-4232

Notes

The authors declare no competing financial interest.

ACKNOWLEDGMENTS

The authors gratefully acknowledge support by the GRK 2450, by the state of Baden-Württemberg through bwHPC (bwUnicluster and JUSTUS, RV bw17D01) and by the Helmholtz Association. T.B. acknowledges support from Slovak Research and Development Agency under the Contract No. APVV-20-0127. The use of the high-performance computing facilities CLARA@UNIBA.SK at Comenius University in Bratislava, services and staff expertise of Centre for Information Technology are also acknowledged.

REFERENCES

(1) Collinge, G.; Yuk, S. F.; Nguyen, M.-T.; Lee, M.-S.; Glezakou, V.-A.; Rousseau, R. Effect of Collective Dynamics and Anharmonicity on Entropy in Heterogenous Catalysis: Building the Case for Advanced Molecular Simulations. *ACS Catal.* **2020**, *10*, 9236−9260.

(2) Studt, F. Grand Challenges in Computational Catalysis. *Front. Catal.* **2021**, *1*, 658965.

(3) Leibfried, G.; Ludwig, W. *Solid State Physics*; Elsevier, 1961; Vol. *12*, pp 275−444.

(4) Hellman, O.; Steneteg, P.; Abrikosov, I. A.; Simak, S. I. Temperature Dependent Effective Potential Method for Accurate Free Energy Calculations of Solids. *Phys. Rev. B* **2013**, *87*, 104111.

(5) Bianco, R.; Errea, I.; Paulatto, L.; Calandra, M.; Mauri, F. Second-Order Structural Phase Transitions, Free Energy Curvature, and Temperature-Dependent Anharmonic Phonons in the Self-Consistent Harmonic Approximation: Theory and Stochastic Implementation. *Phys. Rev. B* **2017**, *96*, 014111.

(6) Knoop, F.; Purcell, T. A. R.; Scheffler, M.; Carbogno, C. Anharmonicity Measure for Materials. *Phys. Rev. Mater.* **2020**, *4*, 083809.

(7) Zacharias, M.; Scheffler, M.; Carbogno, C. Fully Anharmonic Nonperturbative Theory of Vibronically Renormalized Electronic Band Structures. *Phys. Rev. B* **2020**, *102*, 045126.

(8) Moustafa, S. G.; Purohit, A.; Schultz, A. J.; Kofke, D. A. pyHMA: A VASP Post-Processor for Precise Measurement of Crystalline Anharmonic Properties Using Harmonically Mapped Averaging. *Comput. Phys. Commun.* **2021**, *258*, 107554.

(9) Monacelli, L.; Bianco, R.; Cherubini, M.; Calandra, M.; Errea, I.; Mauri, F. The Stochastic Self-Consistent Harmonic Approximation: Calculating Vibrational Properties of Materials with Full Quantum and Anharmonic Effects. *J. Phys.: Condens. Matter* **2021**, *33*, 363001.

(10) Pitzer, K. S.; Gwinn, W. D. Energy Levels and Thermodynamic Functions for Molecules with Internal Rotation I. Rigid Frame with Attached Tops. *J. Chem. Phys.* **1942**, *10*, 428−440.

(11) McClurg, R. B.; Flagan, R. C.; Goddard, W. A., III The Hindered Rotor Density-of-States Interpolation Function. *J. Chem. Phys.* **1997**, *106*, 6675−6680.

(12) Sprowl, L. H.; Campbell, C. T.; Árnadóttir, L. Hindered Translator and Hindered Rotor Models for Adsorbates: Partition Functions and Entropies. *J. Phys. Chem. C* **2016**, *120*, 9719−9731.

(13) Sprowl, L. H.; Campbell, C. T.; Árnadóttir, L. Correction to "Hindered Translator and Hindered Rotor Models for Adsorbates: Partition Functions and Entropies". *J. Phys. Chem. C* **2017**, *121*, 9655−9655.

(14) Pfaendtner, J.; Yu, X.; Broadbelt, L. J. The 1-D Hindered Rotor Approximation. *Theor. Chem. Acc.* **2007**, *118*, 881−898.

(15) Jørgensen, M.; Grönbeck, H. Adsorbate Entropies with Complete Potential Energy Sampling in Microkinetic Modeling. *J. Phys. Chem. C* **2017**, *121*, 7199−7207.

(16) Baron, R.; van Gunsteren, W.; Hünenberger, P. Estimating the Configurational Entropy from Molecular Dynamics Simulations: Anharmonicity and Correlation Corrections to the Quasi-Harmonic Approximation. *Trends Phys. Chem.* **2006**, *11*, 87−122.

(17) Baron, R.; Hünenberger, P. H.; McCammon, J. A. Absolute Single-Molecule Entropies from Quasi-Harmonic Analysis of Microsecond Molecular Dynamics: Correction Terms and Convergence Properties. *J. Chem. Theory Comput.* **2009**, *5*, 3150−3160.

(18) Hellman, O.; Abrikosov, I. A.; Simak, S. I. Lattice Dynamics of Anharmonic Solids from First Principles. *Phys. Rev. B* **2011**, *84*, 180301.

(19) Hellman, O.; Abrikosov, I. A. Temperature-Dependent Effective Third-Order Interatomic Force Constants from First Principles. *Phys. Rev. B* **2013**, *88*, 144301.

(20) Piccini, G.; Sauer, J. Quantum Chemical Free Energies: Structure Optimization and Vibrational Frequencies in Normal Modes. *J. Chem. Theory Comput.* **2013**, *9*, 5038−5045.

(21) Piccini, G.; Sauer, J. Effect of Anharmonicity on Adsorption Thermodynamics. *J. Chem. Theory Comput.* **2014**, *10*, 2479−2487.

(22) Piccini, G.; Alessio, M.; Sauer, J.; Zhi, Y.; Liu, Y.; Kolvenbach, R.; Jentys, A.; Lercher, J. A. Accurate Adsorption Thermodynamics of Small Alkanes in Zeolites. Ab Initio Theory and Experiment for H-Chabazite. *J. Phys. Chem. C* **2015**, *119*, 6128−6137.
(23) Piccini, G.; Alessio, M.; Sauer, J. *Ab Initio* Study of Methanol and Ethanol Adsorption on Brønsted Sites in Zeolite H-MFI. *Phys. Chem. Chem. Phys.* **2018**, *20*, 19964−19970.
(24) Waitt, C.; Miles, A. R.; Schneider, W. F. Adsorbate Free Energies from DFT-Derived Translational Energy Landscapes. *J. Phys. Chem. C* **2021**, *125*, 20331−20342.
(25) Beveridge, D. L.; DiCapua, F. M. Free Energy Via Molecular Simulation: Applications to Chemical and Biomolecular Systems. *Annu. Rev. Biophys. Biophys. Chem.* **1989**, *18*, 431−492.
(26) Frenkel, D.; Smit, B. *Understanding Molecular Simulation: From Algorithms to Applications*, 2nd ed.; Computational Science Series; Academic Press: San Diego, 2002.
(27) Chipot, C., Pohorille, A., Eds. *Free Energy Calculations: Theory and Applications in Chemistry and Biology*; Springer Series in Chemical Physics; Springer: Berlin, 2007; Vol. *86*.
(28) Straatsma, T. P.; Berendsen, H. J. C. Free Energy of Ionic Hydration: Analysis of a Thermodynamic Integration Technique to Evaluate Free Energy Differences by Molecular Dynamics Simulations. *J. Chem. Phys.* **1988**, *89*, 5876−5886.
(29) de Oliveira, C. A. F.; Hamelberg, D.; McCammon, J. A. Coupling Accelerated Molecular Dynamics Methods with Thermodynamic Integration Simulations. *J. Chem. Theory Comput.* **2008**, *4*, 1516−1525.
(30) Leroy, F.; dos Santos, D. J. V. A.; Müller-Plathe, F. Interfacial Excess Free Energies of Solid-Liquid Interfaces by Molecular Dynamics Simulation and Thermodynamic Integration. *Macromol. Rapid Commun.* **2009**, *30*, 864−870.
(31) Pohorille, A.; Jarzynski, C.; Chipot, C. Good Practices in Free-Energy Calculations. *J. Phys. Chem. B* **2010**, *114*, 10235−10253.
(32) Bruckner, S.; Boresch, S. Efficiency of Alchemical Free Energy Simulations. II. Improvements for Thermodynamic Integration. *J. Comput. Chem.* **2011**, *32*, 1320−1333.
(33) de Ruiter, A.; Oostenbrink, C. Efficient and Accurate Free Energy Calculations on Trypsin Inhibitors. *J. Chem. Theory Comput.* **2012**, *8*, 3686−3695.
(34) Moustafa, S. G.; Schultz, A. J.; Kofke, D. A. Very Fast Averaging of Thermal Properties of Crystals by Molecular Simulation. *Phys. Rev. E* **2015**, *92*, 043303.
(35) Moustafa, S. G.; Schultz, A. J.; Zurek, E.; Kofke, D. A. Accurate and Precise *Ab Initio* Anharmonic Free-Energy Calculations for Metallic Crystals: Application to Hcp Fe at High Temperature and Pressure. *Phys. Rev. B* **2017**, *96*, 014117.
(36) Moustafa, S. G.; Schultz, A. J.; Kofke, D. A. Effects of Thermostatting in Molecular Dynamics on Anharmonic Properties of Crystals: Application to Fcc Al at High Pressure and Temperature. *J. Chem. Phys.* **2018**, *149*, 124109.
(37) Vočadlo, L.; Alfè, D. *Ab Initio* Melting Curve of the Fcc Phase of Aluminum. *Phys. Rev. B* **2002**, *65*, 214105.
(38) Grabowski, B.; Ismer, L.; Hickel, T.; Neugebauer, J. *Ab Initio* up to the Melting Point: Anharmonicity and Vacancies in Aluminum. *Phys. Rev. B* **2009**, *79*, 134106.
(39) Glensk, A.; Grabowski, B.; Hickel, T.; Neugebauer, J. Breakdown of the Arrhenius Law in Describing Vacancy Formation Energies: The Importance of Local Anharmonicity Revealed by *AbInitio* Thermodynamics. *Phys. Rev. X* **2014**, *4*, 011018.
(40) Glensk, A.; Grabowski, B.; Hickel, T.; Neugebauer, J. Understanding Anharmonicity in Fcc Materials: From Its Origin to *Ab Initio* Strategies beyond the Quasiharmonic Approximation. *Phys. Rev. Lett.* **2015**, *114*, 195901.
(41) Duff, A. I.; Davey, T.; Korbmacher, D.; Glensk, A.; Grabowski, B.; Neugebauer, J.; Finnis, M. W. Improved Method of Calculating *Ab Initio* High-Temperature Thermodynamic Properties with Application to ZrC. *Phys. Rev. B* **2015**, *91*, 214311.
(42) Habershon, S.; Manolopoulos, D. E. Free Energy Calculations for a Flexible Water Model. *Phys. Chem. Chem. Phys.* **2011**, *13*, 19714.
(43) Rossi, M.; Gasparotto, P.; Ceriotti, M. Anharmonic and Quantum Fluctuations in Molecular Crystals: A First-Principles Study of the Stability of Paracetamol. *Phys. Rev. Lett.* **2016**, *117*, 115702.
(44) Torrie, G. M.; Valleau, J. P. Monte Carlo Free Energy Estimates Using Non-Boltzmann Sampling: Application to the Sub-Critical Lennard-Jones Fluid. *Chem. Phys. Lett.* **1974**, *28*, 578−581.
(45) Torrie, G.; Valleau, J. Nonphysical Sampling Distributions in Monte Carlo Free-Energy Estimation: Umbrella Sampling. *J. Comput. Chem.* **1977**, *23*, 187−199.
(46) Kästner, J. Umbrella Sampling. *WIREs Comput. Mol. Sci.* **2011**, *1*, 932−942.
(47) Carter, E. A.; Ciccotti, G.; Hynes, J. T.; Kapral, R. Constrained Reaction Coordinate Dynamics for the Simulation of Rare Events. *Chem. Phys. Lett.* **1989**, *156*, 472−477.
(48) Ciccotti, G.; Ferrario, M. Blue Moon Approach to Rare Events. *Mol. Simul.* **2004**, *30*, 787−793.
(49) Ciccotti, G.; Kapral, R.; Vanden-Eijnden, E. Blue Moon Sampling, Vectorial Reaction Coordinates, and Unbiased Constrained Dynamics. *ChemPhysChem* **2005**, *6*, 1809−1814.
(50) Rey, J.; Raybaud, P.; Chizallet, C.; Bučko, T. Competition of Secondary versus Tertiary Carbenium Routes for the Type B Isomerization of Alkenes over Acid Zeolites Quantified by Ab Initio Molecular Dynamics Simulations. *ACS Catal.* **2019**, *9*, 9813−9828.
(51) Bennett, C. H. Efficient Estimation of Free Energy Differences from Monte Carlo Data. *J. Comp. Phys.* **1976**, *22*, 245−268.
(52) König, G.; Bruckner, S.; Boresch, S. Unorthodox Uses of Bennett's Acceptance Ratio Method. *J. Comput. Chem.* **2009**, *30*, 1712−1718.
(53) Amsler, J.; Plessow, P. N.; Studt, F.; Bučko, T. Anharmonic Correction to Adsorption Free Energy from DFT-Based MD Using Thermodynamic Integration. *J. Chem. Theory Comput.* **2021**, *17*, 1155−1169.
(54) De Moor, B. A.; Ghysels, A.; Reyniers, M.-F.; Van Speybroeck, V.; Waroquier, M.; Marin, G. B. Normal Mode Analysis in Zeolites: Toward an Efficient Calculation of Adsorption Entropies. *J. Chem. Theory Comput.* **2011**, *7*, 1090−1101.
(55) Uzunova, E. L.; Mikosch, H. Adsorption and Activation of Ethene in Transition Metal Exchanged Zeolite Clinoptilolite: A Density Functional Study. *ACS Catal.* **2013**, *3*, 2759−2767.
(56) Wang, C.-M.; Brogaard, R. Y.; Xie, Z.-K.; Studt, F. Transition-State Scaling Relations in Zeolite Catalysis: Influence of Framework Topology and Acid-Site Reactivity. *Catal. Sci. Technol.* **2015**, *5*, 2814−2820.
(57) Kundu, A.; Piccini, G.; Sillar, K.; Sauer, J. Ab Initio Prediction of Adsorption Isotherms for Small Molecules in Metal−Organic Frameworks. *J. Am. Chem. Soc.* **2016**, *138*, 14047−14056.
(58) De Moor, B. A.; Reyniers, M.-F.; Gobin, O. C.; Lercher, J. A.; Marin, G. B. Adsorption of C2-C8 n-Alkanes in Zeolites. *J. Phys. Chem. C* **2011**, *115*, 1204−1219.
(59) Su, Y.-Q.; Wang, Y.; Liu, J.-X.; Filot, I. A.; Alexopoulos, K.; Zhang, L.; Muravev, V.; Zijlstra, B.; Vlachos, D. G.; Hensen, E. J. Theoretical Approach To Predict the Stability of Supported Single-Atom Catalysts. *ACS Catal.* **2019**, *9*, 3289−3297.
(60) Tuckerman, M. E. *Statistical Mechanics: Theory and Molecular Simulation*; Oxford University Press: Oxford, 2010.
(61) Jensen, F. *Introduction to Computational Chemistry*, 2nd ed.; John Wiley & Sons: Chichester, England, 2007.
(62) Wilson, E. B.; Decius, J. C.; Cross, P. C. *Molecular Vibrations: The Theory of Infrared and Raman Vibrational Spectra*; Dover Publications: New York, 1980.
(63) Wilson, E. B. Some Mathematical Methods for the Study of Molecular Vibrations. *J. Chem. Phys.* **1941**, *9*, 76−84.
(64) Ryckaert, J.-P.; Ciccotti, G.; Berendsen, H. J. Numerical Integration of the Cartesian Equations of Motion of a System with Constraints: Molecular Dynamics of n-Alkanes. *J. Comput. Phys.* **1977**, *23*, 327−341.
(65) Baker, J.; Kessi, A.; Delley, B. The Generation and Use of Delocalized Internal Coordinates in Geometry Optimization. *J. Chem. Phys.* **1996**, *105*, 192−212.

(66) Andzelm, J.; King-Smith, R.; Fitzgerald, G. Geometry Optimization of Solids Using Delocalized Internal Coordinates. *Chem. Phys. Lett.* **2001**, *335*, 321−326.
(67) Bučko, T.; Hafner, J.; Ángyán, J. G. Geometry Optimization of Periodic Systems Using Internal Coordinates. *J. Chem. Phys.* **2005**, *122*, 124508.
(68) Bučko, T. Transition State Optimization of Periodic Systems Using Delocalized Internal Coordinates. *Theor. Chem. Acc.* **2018**, *137*, 164.
(69) Bučko, T.; Chibani, S.; Paul, J.-F.; Cantrel, L.; Badawi, M. Dissociative Iodomethane Adsorption on Ag-MOR and the Formation of AgI Clusters: An Ab Initio Molecular Dynamics Study. *Phys. Chem. Chem. Phys.* **2017**, *19*, 27530−27543.
(70) Sprik, M.; Ciccotti, G. Free Energy from Constrained Molecular Dynamics. *J. Chem. Phys.* **1998**, *109*, 7737−7744.
(71) Cnudde, P.; De Wispelaere, K.; Vanduyfhuys, L.; Demuynck, R.; Van der Mynsbrugge, J.; Waroquier, M.; Van Speybroeck, V. How Chain Length and Branching Influence the Alkene Cracking Reactivity on H-ZSM-5. *ACS Catal.* **2018**, *8*, 9579−9595.
(72) Rey, J.; Bignaud, C.; Raybaud, P.; Bučko, T.; Chizallet, C. Dynamic Features of Transition States for β-Scission Reactions of Alkenes over Acid Zeolites Revealed by AIMD Simulations. *Angew. Chem.* **2020**, *132*, 19100−19104.
(73) Kresse, G.; Hafner, J. *Ab Initio* Molecular Dynamics for Open-Shell Transition Metals. *Phys. Rev. B* **1993**, *48*, 13115−13118.
(74) Kresse, G.; Hafner, J. *Ab Initio* Molecular-Dynamics Simulation of the Liquid-Metal−Amorphous-Semiconductor Transition in Germanium. *Phys. Rev. B* **1994**, *49*, 14251−14269.
(75) Kresse, G.; Furthmüller, J. Efficiency of Ab-Initio Total Energy Calculations for Metals and Semiconductors Using a Plane-Wave Basis Set. *Comput. Mater. Sci.* **1996**, *6*, 15−50.
(76) Kresse, G.; Furthmüller, J. Efficient Iterative Schemes for *Ab Initio* Total-Energy Calculations Using a Plane-Wave Basis Set. *Phys. Rev. B* **1996**, *54*, 11169−11186.
(77) Blöchl, P. E. Projector Augmented-Wave Method. *Phys. Rev. B* **1994**, *50*, 17953−17979.
(78) Kresse, G.; Joubert, D. From Ultrasoft Pseudopotentials to the Projector Augmented-Wave Method. *Phys. Rev. B* **1999**, *59*, 1758−1775.
(79) Perdew, J. P.; Burke, K.; Ernzerhof, M. Generalized Gradient Approximation Made Simple. *Phys. Rev. Lett.* **1996**, *77*, 3865−3868.
(80) Grimme, S.; Antony, J.; Ehrlich, S.; Krieg, H. A Consistent and Accurate *Ab Initio* Parametrization of Density Functional Dispersion Correction (DFT-D) for the 94 Elements H-Pu. *J. Chem. Phys.* **2010**, *132*, 154104.
(81) Bučko, T.; Hafner, J.; Lebègue, S.; Ángyán, J. G. Improved Description of the Structure of Molecular and Layered Crystals: Ab Initio DFT Calculations with van Der Waals Corrections. *J. Phys. Chem. A* **2010**, *114*, 11814−11824.
(82) Monkhorst, H. J.; Pack, J. D. Special Points for Brillouin-zone Integrations. *Phys. Rev. B* **1976**, *13*, 5188−5192.
(83) Plessow, P. N. Efficient Transition State Optimization of Periodic Structures through Automated Relaxed Potential Energy Surface Scans. *J. Chem. Theory Comput.* **2018**, *14*, 981−990.
(84) Hratchian, H. P.; Schlegel, H. B. Following Reaction Pathways Using a Damped Classical Trajectory Algorithm. *J. Phys. Chem. A* **2002**, *106*, 165−169.
(85) Bučko, T. Ab Initio calculations of Free-Energy Reaction Barriers. *J. Phys.: Condens. Matter* **2008**, *20*, 064211.
(86) Andersen, H. C. Molecular Dynamics Simulations at Constant Pressure and/or Temperature. *J. Chem. Phys.* **1980**, *72*, 2384−2393.
(87) Réocreux, R.; Michel, C.; Fleurat-Lessard, P.; Sautet, P.; Steinmann, S. N. Evaluating Thermal Corrections for Adsorption Processes at the Metal/Gas Interface. *J. Phys. Chem. C* **2019**, *123*, 28828−28835.
(88) Schiferl, S. K.; Wallace, D. C. Statistical Errors in Molecular Dynamics Averages. *J. Chem. Phys.* **1985**, *83*, 5203−5209.
(89) Shklov, N. Simpson's Rule for Unequally Spaced Ordinates. *Am. Math. Mon.* **1960**, *67*, 1022.
(90) Press, W. H., Ed. *Numerical Recipes: The Art of Scientific Computing*, 3rd ed.; Cambridge University Press: Cambridge, UK, 2007.
(91) Reed, B. C. Numerically Integrating Irregularly-spaced (x, y) Data. *Math. Enthus.* **2014**, *11* (3), 643−648.
(92) Branduardi, D.; Gervasio, F. L.; Parrinello, M. From A to B in Free Energy Space. *J. Chem. Phys.* **2007**, *126*, 054103.
(93) Bučko, T.; Gešvandtnerová, M.; Rocca, D. Ab Initio Free Energy Calculations at Multiple Electronic Structure Levels Made Affordable: An Effective Combination of Perturbation Theory and Machine Learning. *J. Chem. Theory Comput.* **2020**, *16*, 6049−6060.
(94) Flyvbjerg, H.; Petersen, H. G. Error Estimates on Averages of Correlated Data. *J. Chem. Phys.* **1989**, *91*, 461−466.
(95) Herzog, B.; Chagas da Silva, M.; Casier, B.; Badawi, M.; Pascale, F.; Bučko, T.; Lebègue, S.; Rocca, D. Assessing the Accuracy of Machine Learning Thermodynamic Perturbation Theory: Density Functional Theory and Beyond. *J. Chem. Theory Comput.* **2022**, *18*, 1382−1394.
(96) Li, P.; Jia, X.; Pan, X.; Shao, Y.; Mei, Y. Accelerated Computation of Free Energy Profile at ab Initio Quantum Mechanical/Molecular Mechanics Accuracy via a Semi-Empirical Reference Potential. I. Weighted Thermodynamics Perturbation. *J. Chem. Theory Comput.* **2018**, *14*, 5583−5596.
(97) Jinnouchi, R.; Lahnsteiner, J.; Karsai, F.; Kresse, G.; Bokdam, M. Phase Transitions of Hybrid Perovskites Simulated by Machine-Learning Force Fields Trained on the Fly with Bayesian Inference. *Phys. Rev. Lett.* **2019**, *122*, 225701.
(98) Jinnouchi, R.; Miwa, K.; Karsai, F.; Kresse, G.; Asahi, R. On-the-Fly Active Learning of Interatomic Potentials for Large-Scale Atomistic Simulations. *J. Phys. Chem. Lett.* **2020**, *11*, 6946−6955.
(99) Bannwarth, C.; Caldeweyher, E.; Ehlert, S.; Hansen, A.; Pracht, P.; Seibert, J.; Spicher, S.; Grimme, S. Extended Tight-binding Quantum Chemistry Methods. *WIREs Comput. Mol. Sci.* **2021**, *11*, No. e1493.
(100) Blöndal, K.; Sargsyan, K.; Bross, D. H.; Ruscic, B.; Goldsmith, C. F. Adsorbate Partition Functions via Phase Space Integration: Quantifying the Effect of Translational Anharmonicity on Thermodynamic Properties. *J. Phys. Chem. C* **2021**, *125*, 20249−20260.
(101) Bartók, A. P.; Kondor, R.; Csányi, G. On Representing Chemical Environments. *Phys. Rev. B* **2013**, *87*, 184115.
(102) Rupp, M.; Tkatchenko, A.; Müller, K.-R.; von Lilienfeld, O. A. Fast and Accurate Modeling of Molecular Atomization Energies with Machine Learning. *Phys. Rev. Lett.* **2012**, *108*, 058301.